J Nanopart Res (2017) 19:50
DOI 10.1007/s11051-017-3759-0

RESEARCH PAPER

Molecular beam epitaxial growth of oriented and uniform $Ge_2Sb_2Te_5$ nanoparticles with compact dimensions

Beining Zheng · Yu Sun · Jie Wu · Long Yuan · Xiaofeng Wu · Keke Huang · Shouhua Feng

Received: 29 August 2016 / Accepted: 24 January 2017

Abstract The scaling-down of phase change memory cell is critical to achieve high-performance and high-density memory devices. Herein, we report that $Ge_2Sb_2Te_5$ nanoparticles along the [1 1 1] direction were synthesized without templates or etching in a molecular beam epitaxy system. Under non-stoichiometric Ge:Sb:Te beam ratio condition, the growth of high-density $Ge_2Sb_2Te_5$ nanoparticles was achieved by Zn-doping. The average diameter of the nanoparticles is 8 nm, and the full width at half maximum of the size distribution is 2.7 nm. Our results suggest that the size and shape modifications of $Ge_2Sb_2Te_5$ nanoparticles could be induced by Zn-doping which influences the nucleation in the growth process. In addition, the bonding states of Zn and Te verified by X-ray photoelectron spectroscopy proved that Zn atoms located in the $Ge_2Sb_2Te_5$ matrix. This approach exemplified here can be applied to the sub-20 nm phase change memory devices and may also be extendable to be served in the design and development of more materials with phase transitions.

Keywords Nanoparticles · Ge2Sb2Te5 · Molecular beam epitaxy · Memory device applications

B. Zheng · Y. Sun · J. Wu · L. Yuan · X. Wu · K. Huang · S. Feng (✉)
State Key Laboratory of Inorganic Synthesis and Preparative Chemistry, College of Chemistry, Jilin University, Changchun 130012, People's Republic of China
e-mail: shfeng@jlu.edu.cn

Introduction

Multicomponent chalcogenides could be seen as phase-change random access memory (PCRAM) due to the thermally induced and reversible crystalline-to-amorphous phase transitions which associated with distinct property states (Meijer 2008; Kolobov et al. 2004). Chalcogenide compounds located in the GeTe, SbTe, ternary Ge:Sb:Te, and their alloy show distinguishable phases, excellent scalability, and nonvolatility (Lencer et al. 2011). However, their wide spread commercialization is mostly constrained by a relatively high-programming current (0.1–0.5 mA) and power (~0.5 mW) (Burr et al. 2010; Wong et al. 2010). Their writing current and the power consumption both diminish with a volume decrease of phase change material (Lencer et al. 2011; Burr et al. 2010; Pirovano et al. 2004). The size effect motivates the investigation into the improvements of phase change properties with material dimensions.

$Ge_2Sb_2Te_5$ (GST) is a representative commercially composition with a high switching rate and extremely good reversibility owing to its rocksalt structure (Orava et al. 2012). The potential for GST to exhibit promising phase change properties in the nanometer regimes has prompted recent reports on thin films (2 nm) (Simpson et al. 2010) and nanowires (20 to 200 nm) (Lee et al. 2007a, b; Jung et al. 2006). Nanoparticles, in particular, can be a feasible approach of building memory devices proportionately to the particle size, and allowing device functionality to be assembled with the same structure (Tseng et al. 2006; Nie et al. 2010). The common

Published online: 04 February 2017

synthetic strategies are focused on the preparation of relatively large size particles (100 nm and 100 μm) by employing sputter deposition and electron-beam lithographic method (Raoux et al. 2007). Only few efforts were devoted to synthesize dimensionally controlled GST nanoparticles in the size range of sub-100 nm, which will allow a continued scalability for ultra-high density PCRAM while retaining nonvolatility (Lee et al. 2007a). The GST nanoparticles with varying sizes of 200 nm to 2 μm were prepared by ICP etching and UV nano-imprint lithography (Yang et al. 2007). The size of GST nanoparticles which synthesized by a self-assembled polymer lithography was less than 15 nm in diameter with 40 nm spacing (Zhang et al. 2008). And amorphous GST nanoparticles containing multiple compositions, with a size distribution of 4 to 30 nm at a nominal 15 nm, was synthesized by pulsed-laser ablation (Yoon et al. 2006; Choi et al. 2005). The design of PCRAM device with fascinating physical features requires the high-quality, well-defined GST nanoparticles with smaller diameters. However, experimental progress in the field is limited by the ability to reduce the size regime to sub-lithographic length scales.

Molecular beam epitaxy is an important technology used to investigate the structure of nanoparticles, especially the one with a diameter less than 10 nm. It has not been developed for the growth of GST particles in a nanometer scale so far. In this paper, GST nanoparticles on Si (1 1 1) substrates were grown by molecular beam epitaxy. The high-density particles' size is smaller than most structures obtained by lithography method. Non-stoichiometry ratio was adopted during the processing. Zn-doping could remarkably develop the growth, resulting in the high-density, uniform-size GST nanoparticles dispersing on the surfaces. The growth was neither done without any template masks or etching which pose the risk of unacceptable damages on the material surfaces leading to degrading properties. It may be a promising solution to scale down the size of phase change materials without using high-cost lithographic tools.

Experimental

The growth of GST nanoparticles was carried out on Si (1 1 1) substrates in an SVTA MBE apparatus under a chamber pressure 8×10^{-11} Torr. The MBE system was equipped with two standard effusion cells for Ge and Zn, and two valved cracker cell for Sb and Te. Prior to growth, Si (1 1 1) wafers were chemically cleaned using standard Shiraki clean procedures (Kern 1990). The wafers were dried with N_2 blow and immediately loaded into the load-lock chamber. A high-quality (7 × 7) reconstructed surface was obtained by annealing the substrates at 800 °C for 15 min (De Renzi et al. 2002). The Ge:Sb:Te beam equivalent pressure ratio was fixed at 1:1:2 at appropriate evaporation temperatures. Ge and Sb rich conditions were performed in order to rule out the formation of GST film. Zn evaporation temperature was set 275 °C for doping. Considering the case of GST film whose growth temperature window was narrow (Katmis et al. 2011), the substrate temperature was 200 °C for a continuous epitaxial crystallization. Homogeneously Zn-doped sample was obtained by Ge, Sb, Te, and Zn sources impinging the substrate constantly. In addition, the sample with 50% doping amount was achieved by controlling Zn tube shutter to open and close with 1-min interval time. All growth process adopted same growth time. Furthermore, undoped GST with equivalent thickness was grown to contrast the performance of Zn doping.

The structural analysis of as-grown samples was examined by a Rigaku Ultima IV X-ray diffractometer (XRD) with Cu K_{α} radiation. Surface morphology images were acquired by scanning electron microscope (SEM) with an FEI Helios NanoLab 600I microscope operating at 10 kV. The Seiko SPA400 SPIWIN atomic force microscope (AFM) was used to identify the topography. High-resolution transmission electron microscopy (HRTEM) images were obtained by an FEI Tecnai G2 S-Twin F20 electron microscope. The particle size distributions and average diameters were measured and calculated by the software Nano Measurer 1.2. X-ray photoelectron spectroscopy (XPS) data were collected by a Thermo Scientific ESCALAB 250Xi XPS system to determine the chemical bond type in the Zn-doped GST nanoparticle.

Results

Figure 1 presents typically normalized XRD patterns of the undoped sample (c) and the two doped ones (a) and (b). The two peaks at 25.6° and 52.3° are attributed to (1 1 1) and (2 2 2) plane of GST reflections in cubic phase (Inorganics 54–0484, $Fm\bar{3}m$) (Thelander et al. 2014).

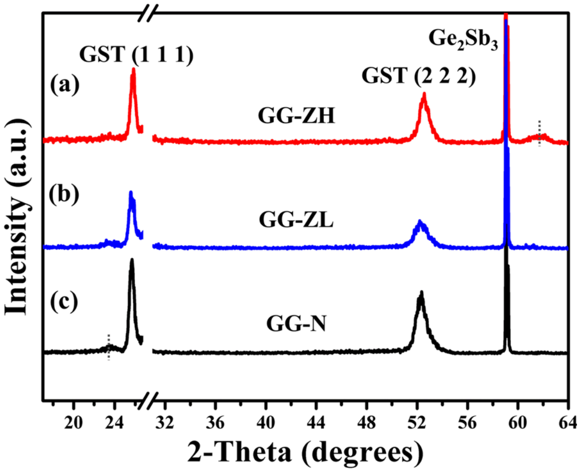

Fig. 1 The XRD patterns of each sample. **a** Zn-doped with high content sample (GG-ZH). **b** Zn-doped with low content sample (GG-ZL). **c** Undoped Ge-Sb-Te composite sample (GG-N). A high intensity peak at 28.4° for Si (1 1 1) orientation is hidden

The sharp peak lied at 59° is corresponding to the Ge_2Sb_3 alloy phase (Inorganics 37–0970, *I4mm*) due to Ge and Sb rich flux which indicates that two eutectic compositions contained Ge_2Sb_3 alloy and GST were deposited on Si (1 1 1) substrates. The above three samples are named as GG-N (Ge_2Sb_3-GST none doped), GG-ZH (Ge_2Sb_3-GST Zn doped with high content), and GG-ZL (Ge_2Sb_3-GST Zn doped with low content), respectively. XRD peaks of the samples gradually shifts to high two-theta angle as Zn doping content rising. Additionally, a weak polycrystalline orientation appearing at 23.5° in Fig. 1c belongs to Sb metal. Since Zn is doped into the matrix, there is a peak of SbZn appearing at 61.5° (Fig. 1a) manifesting the reaction of Zn and Sb.

HRTEM was carried out to further understand the structural details of the nanoparticles. The face centered cubic (fcc) GST has a rocksalt structure, with the space group $Fm\overline{3}m$. Figure 2a shows the typical image of GG-N mixture. The adjacent interplanar spacing is 3.11 Å corresponding to the closest (0 0 2) plane of fcc structure

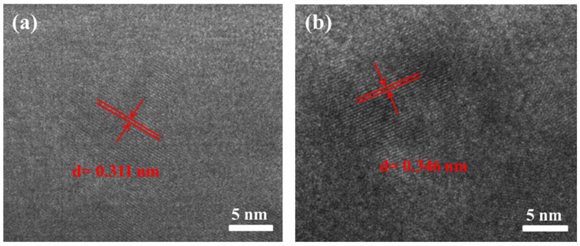

Fig. 2 HRTEM images of **a** GG-N and **b** GG-ZL samples

dominant component Ge_2Sb_3. The distance is 3.46 Å in the GG-ZL sample (Fig. 2b) in accordance with the fcc GST (1 1 1) lattice plane.

Figure 3 shows topography of GST nanoparticles deposited on Si (1 1 1) substrates. The morphologies of Zn-doped samples are distinct from the undoped ones. In comparison with the undoped sample (Fig. 3a), numbers of nanoparticles emerges on the surfaces with the introduction of Zn dopant as shown in Fig. 3c, e. The composition of the nanoparticles is identified as GST by the above results. Particle of small size usually corresponds to broad XRD peak owing to the high specific surface area and the poor lattice arrangement at the particle surface (Wang et al. 2013). The measured root mean square values are 1.131 nm of GG-N, 1.601 nm of GG-ZL, and 1.699 nm of GG-ZH as shown in the AFM images (Fig. 3b, d, f).

The size distributions of GST particles were compiled. The statistical histogram of the size distribution is exhibited in Fig. 4. The diameters of the nanoparticles

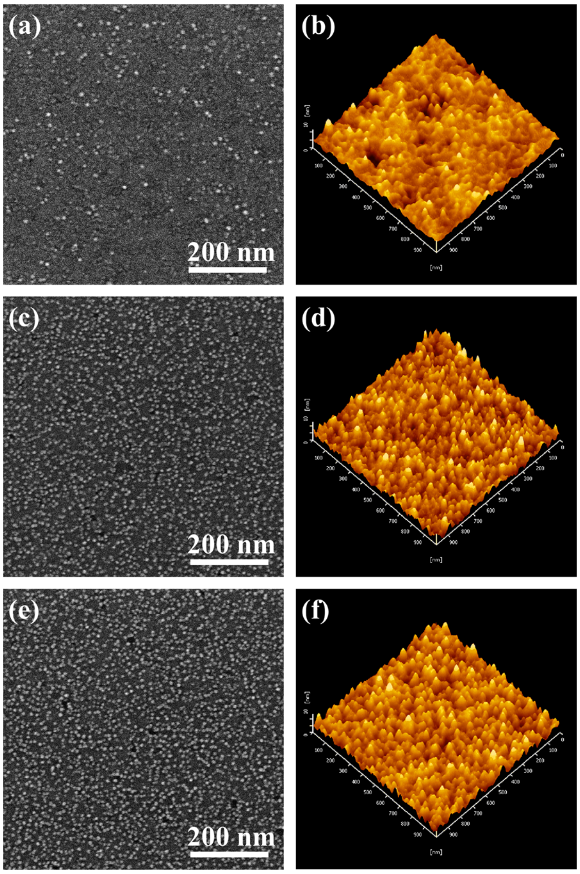

Fig. 3 SEM images of the samples **a** GG-N, **c** GG-ZL, **e** GG-ZH. The AFM morphologies of corresponding samples **b**, **d**, and **f**

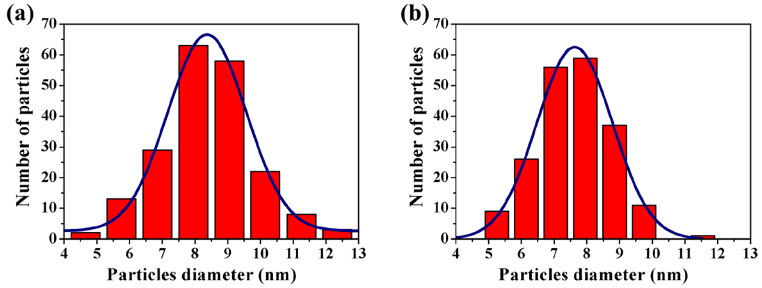

Fig. 4 Statistical size distribution for GST nanoparticles of **a** GG-ZL and **b** GG-ZH samples

are ranging from 5 to 13 nm, and the average sizes are 8.39 nm of GG-ZL and 7.62 nm of GG-ZH. The full width at half maximum of the size distribution for GG-ZL sample is 2.72 nm, and for GG-ZH is 2.82 nm.

The bonding states of GST nanoparticles were investigated by XPS in order to confirm the influence of Zn dopant. The Sb 3d pattern of GG-N is depicted in Fig. 5a. The asymmetric peak located at 530.90 eV is formed by O 1 s and Sb $3d_{5/2}$ overlapped with each other (Barick et al. 2010), and it can be divided into two portions. The peak at 530.65 eV is corresponding to Sb $3d_{5/2}$, and the remainder (O 1 s) should be the surface oxide that was formed on the layer during transfer with exposure to air. The set of Sb 3d peaks at a higher energy ($3d_{3/2}$ 540.00 eV and $3d_{5/2}$ 530.65 eV) belongs to GST nanoparticle phase. Meanwhile, the lower ones ($3d_{3/2}$ 537.75 eV and $3d_{5/2}$ 528.40 eV) belong to the Ge_2Sb_3 alloy. The XPS spectrum of Zn 2p region for GG-ZH is shown in Fig. 5b. The peak centered at 1021.79 eV is assigned to the Zn $2p_{3/2}$. Figure 5c displays the Te 3d spectra of the composites with different Zn-doped concentrations. It is obvious that the peaks ($3d_{3/2}$~582.6 eV and $3d_{5/2}$~572.4 eV) related to the GST shifted to the lower binding energy as the Zn concentration increase.

Discussion

Our results show the GST and Ge_2Sb_3 alloy was deposited on substrate surface. Particle of small size usually corresponds to broad XRD peak owing to the high specific surface area and the poor lattice arrangement at the particle surface (Wang et al. 2013). So based on the XRD and SEM results, the composition of the nanoparticles is identified as GST. And in the eutectic mixture, GST nanoparticles are embedded in the Ge_2Sb_3 alloy like plum-pudding type. After Zn doping, the change of surface morphologies give a qualitative picture that the isolated GST nanoparticles could significantly emerge from the eutectic mixture. In terms of size and density, the nanoparticles are superior to the one which were prepared by pulsed-laser ablation (Yoon et al. 2006). Base on the above phenomena, the growth process can be summarized as follows. In this case, due to the excess of Ge and Sb flux condition, Ge would bond with Sb to form Ge_2Sb_3 alloy. The Ge_2Sb_3 alloy was deposited on the substrate with GST at the same time. Thus, the plum-pudding type GST nanoparticles were fabricated successfully. This eutectic mixture played a key role in a uniformly dispersed surface anchorage of the GST nanostructure.

In comparison with undoped sample, the density of GST nanoparticles increases significantly with Zn-doping (Fig. 3). With the increase of Zn dopant amount, the XRD peaks of GST gradually shift to high two-theta angle, and the XRD results show the symmetry structure of GST cubic unit cell broken along the [1 1 1] direction. The Zn $2p_{3/2}$ peak position is 0.7 higher than that of the metal Zn-Zn binding energy (Zeng et al. 2014). It implies that Zn is bond with a higher electronegativity and successfully incorporated into the composites. Because the negative shift in the binding energy is caused by the decrease in the electronegativity of neighboring atoms (Wang et al. 2007), it can be concluded by the Td 3d peaks shift that Zn atoms subsequently form Zn-Te bonds after the doping process. As we know, the formation of crystal nucleation and the growth of nucleation are the procedure that the nanoparticles growth needs to go through. According to these results, we surmise that the density increase is attributed to Zn dopant, which incorporate in and interacting with the GST host matrix and further influence the nucleation in GST nanoparticle growth process. On the basis of S. R. Elliott's simulation work (Skelton et al. 2012), Zn atoms prefer tetrahedral coordination, locating near to voids and adopting a four-coordinate defective-octahedral geometry in the GST crystalline phase (Fig. 6a, b), which will destroy the octahedral symmetry of GST cubic unit cell. Moreover,

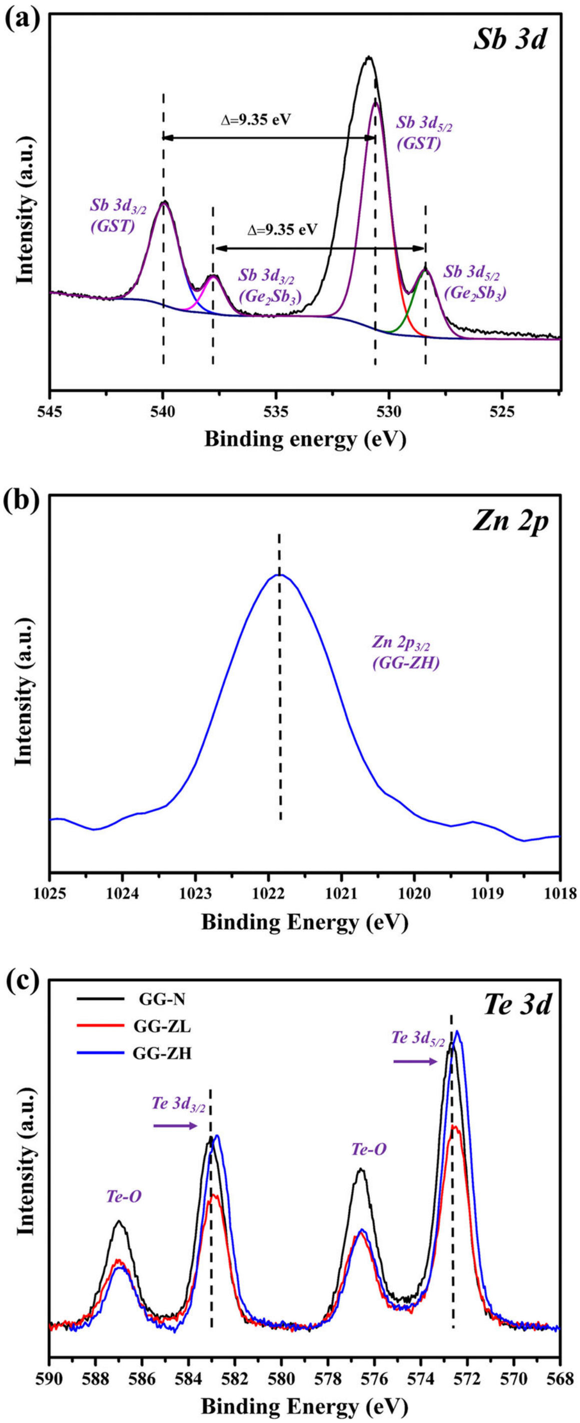

Fig. 5 Typical **a** Sb 3d and **b** Zn 2p XPS spectra of GG-N, **c** Te 3d spectra of GG-N (*black*), GG-ZL (*red*), and GG-ZH (*blue*)

this coordination configuration is lower in energy than the undoped one. Therefore, the Zn dopant could decrease the activation barrier of GST nanoparticle nucleation, and facilitate the growth of the GST nanoparticles. On the other hand, the crystalline material is long-range ordered, while the amorphous material is short-range ordered. For amorphous Ge_2Sb_3 alloy, coordination with doped Zn atom would destroy some short ordered ranges which lead to the structure more disorder, and also obstruct the atom movement. Compared to the crystalline, the amorphous Ge_2Sb_3 alloy needs more energy to drive the bonds breaking and the atoms moving. Therefore, the Zn dopant has less influence on the Ge_2Sb_3 alloy. As a result, high-density GST nanoparticles are exposed at the mixture surface. Figure 6c is a schematic diagram explaining the experimental process in this study.

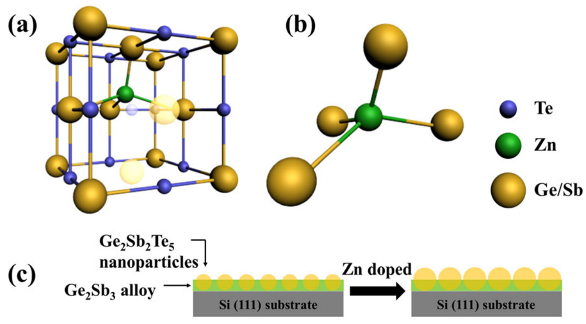

Fig. 6 **a** Structure model of Zn-doped GST. **b** An expanded view of the local atomic geometries around the Zn atoms. **c** Schematic of the growth pattern followed in this study

Many crucial attributes of GST significantly rely on the length of line cells (Lankhorst et al. 2005). Because electron-beam and extreme ultraviolet sources have limited capable of resolving patterns with dimensions of 20 nm (Stoykovich and Nealey 2006), the size of the nano cell that obtained from the photolithography cannot be scaled to less than 20 nm length, which is demanded by the future ideal characteristics. Considering the size of the GST nanoparticles in this case, the method of growth GST nanoparticles provides an approach to overcome the photolithography obstacle. Furthermore, the lithographic process has many complicated steps (Grosse et al. 2001). However, the growth in our experiment is done in one step without any template masks or etching. So the simple and economic is another advantage compared to the photolithography.

The writing current energy and threshold voltage for Ge-Sb nanowire are measured as ~1.6 mW and ~4 V (Jung et al. 2009), these are obviously distinct from the GST nanowire (1.5 mW and 3 V) (Lee et al. 2008; Lankhorst et al. 2005). The separated phase-change process can be obtained through adopting the designated value duration of threshold voltage/current pulse. On the other hand, the phase transformation process is accompanied by the atomic rearrangement and atoms movements (Da Silva et al. 2009; Privitera et al. 2007), and a distorted octahedral atomic arrangement of Ge-Sb has been observed in the GST phase change between the amorphous and metastable phases by atomic-resolution Cs-corrected STEM study (Lotnyk et al. 2016). Many studies have found that when the GST is adjacent to the similarity component materials, such as Sb, GeTe, nitrogen-doped GST, and mixed phase GST (Hu et al. 2015; Hu et al. 2012; Tan et al. 2013; Privitera et al. 2013), the adjacent structure is beneficial to the atom movements, and the phase transition properties are improved consequently. Therefore, the Ge_2Sb_3 alloy matrix would offer a great opportunity to boost GST nanoparticle phase-change properties. So the memory storage function might be realized in the GST nanoparticle and Ge_2Sb_3 alloy hybrid structure, but these discussions still need a direct proof via electrical characteristics.

Conclusions

Oriented and uniform GST nanoparticles were successfully prepared on Si (1 1 1) substrates by molecular beam epitaxy. Under non-stoichiometric Ge:Sb:Te beam ratio condition, the growth of high-density GST nanoparticles was achieved by Zn-doping in one simple step. The approach is more effective and flexible compared with lithography. The epitaxy of GST nanoparticles is oriented along [1 1 1] directions, and the grain average diameter is 8 nm, and the full width at half maximum of the size distribution is 2.7 nm. In addition, the chemical state of Zn atoms incorporated into the cubic GST lattices is classified as the formation of Zn-Te bond by XPS spectra. These results are highly meaningful in which the method is possible to be an approach to overcome the diffraction limitation of optical in the lithography process and open interesting opportunities for further shrinking the memory device dimensions.

Acknowledgements This study was funded by the National Natural Science Foundation of China (Grants 21427802, 21131002, and 21201075).

Compliance with ethical standards

Conflict of interest The authors declare that they have no conflict of interest.

References

Barick KC, Aslam M, Dravid VP, Bahadur D (2010) Controlled fabrication of oriented co-doped ZnO clustered nanoassemblies. J Colloid Interface Sci 349:19–26. doi:10.1016/j.jcis.2010.05.036

Burr GW et al (2010) Phase change memory technology. J Vac Sci Technol B 28:223–262. doi:10.1116/1.3301579

Choi HS, Seol KS, Takeuchi K, Fujita J, Ohki Y (2005) Synthesis of size- and structure-controlled $Ge_2Sb_2Te_5$ nanoparticles. Jpn J Appl Phys Part 1 - Regul Pap Brief Commun Rev Pap 44:7720–7722. doi:10.1143/jjap.44.7720

Da Silva JL, Walsh A, Wei SH, Lee H (2009) Atomistic origins of the phase transition mechanism in $Ge_2Sb_2Te_5$. J Appl Phys 106:113509. doi:10.1063/1.3264883

De Renzi V, Biagi R, del Pennino U (2002) Study of the transition from the ideal Si(111)-H(1 × 1) surface to the (7 × 7) reconstruction by HREELS, UPS and LEED. Surf Sci 497:247–253. doi:10.1016/s0039-6028(01)01647-8

Grosse A, Grewe M, Fouckhardt H (2001) Deep wet etching of fused silica glass for hollow capillary optical leaky waveguides in microfluidic devices. J Micromech Microe 11:257. doi:10.1088/0960-1317/11/3/315

Hu Y, Sun M, Song S, Song Z, Zhai J (2012) Multi-step resistance memory behavior in $Ge_2Sb_2Te_5$/GeTe stacked chalcogenide films. Integr Ferroelectr 140:8–15. doi:10.1080/10584587.2012.741367

Hu Y, Zou H, Zhang J, Xue J, Sui Y, Wu W, Li Y, Zhu X, Song S, Song Z (2015) $Ge_2Sb_2Te_5$/Sb superlattice-like thin film for high speed phase change memory application. Appl Phys Lett 107:263105. doi:10.1063/1.4939149

Jung Y, Lee SH, Ko DK, Agarwal R (2006) Synthesis and characterization of $Ge_2Sb_2Te_5$ nanowires with memory switching effect. J Am Chem Soc 128:14026–14027. doi:10.1021/ja065938s

Jung Y, Yang CY, Lee SH, Agarwal R (2009) Phase-change Ge − Sb nanowires: synthesis, memory switching, and phase-instability. Nano Lett 9:2103–2108. doi:10.1021/nl900620n

Katmis F et al (2011) Insight into the growth and control of single-crystal layers of Ge-Sb-Te phase-change material. Cryst Growth Des 11:4606–4610. doi:10.1021/cg200857x

Kern W (1990) The evolution of silicon wafer cleaning technology. J Electrochem 137:1887–1892. doi:10.1149/1.2086825

Kolobov AV, Fons P, Frenkel AI, Ankudinov AL, Tominaga J, Uruga T (2004) Understanding the phase-change mechanism of rewritable optical media. Nat Mater 3:703–708. doi:10.1038/nmat1215

Lankhorst MHR, Ketelaars BW, Wolters RAM (2005) Low-cost and nanoscale non-volatile memory concept for future silicon chips. Nat Mater 4:347–352. doi:10.1038/nmat1350

Lee SH, Jung Y, Agarwal R (2007b) Highly scalable non-volatile and ultra-low-power phase-change nanowire memory. Nat Nanotechnol 2:626–630. doi:10.1038/nnano.2007.291

Lee H, Hong SH, Yang KY, Jung GY (2007a) Fabrication of $Ge_2Sb_2Te_5$ based PRAM device at 60 nm scale by using UV nanoimprint lithography. Microelectron Eng 84:573–576. doi:10.1016/j.mee.2006.11.009

Lee SH, Jung Y, Chung HS, Jennings AT, Agarwal R (2008) Comparative study of memory-switching phenomena in phase change GeTe and $Ge_2Sb_2Te_5$ nanowire devices. Phys E 40:2474–2480. doi:10.1016/j.physe.2007.09.171

Lencer D, Salinga M, Wuttig M (2011) Design rules for phase-change materials in data storage applications. Adv Mater 23: 2030–2058. doi:10.1002/adma.201004255

Lotnyk A, Bernütz S, Sun X, Ross U, Ehrhardt M, Rauschenbach B (2016) Real-space imaging of atomic arrangement and vacancy layers ordering in laser crystallised $Ge_2Sb_2Te_5$ phase change thin films. Acta Mater 105:1–8. doi:10.1016/j.actamat.2015.12.010

Meijer GI (2008) Materials science—who wins the nonvolatile memory race? Science 319:1625–1626. doi:10.1126/science.1153909

Nie ZH, Petukhova A, Kumacheva E (2010) Properties and emerging applications of self-assembled structures made from inorganic nanoparticles. Nat Nanotechnol 5:15–25. doi:10.1038/nnano.2009.453

Orava J, Greer AL, Gholipour B, Hewak DW, Smith CE (2012) Characterization of supercooled liquid $Ge_2Sb_2Te_5$ and its crystallization by ultrafast-heating calorimetry. Nat Mater 11:279–283. doi:10.1038/nmat3275

Pirovano A, Lacaita AL, Pellizzer F, Kostylev SA, Benvenuti A, Bez R (2004) Low-field amorphous state resistance and threshold voltage drift in chalcogenide materials. IEEE Trans Electron Devices 51:714–719. doi:10.1109/ted.2004.825805

Privitera S, Lombardo S, Bongiorno C, Rimini E, Pirovano A (2007) Phase change mechanisms in $Ge_2Sb_2Te_5$. J Appl Phys 102:3516. doi:10.1063/1.2752111

Privitera S, Garozzo C, Alberti A, Perniola L, De Salvo B (2013) Mixed phase $Ge_2Sb_2Te_5$ thin films with temperature independent resistivity. AIP Adv 3:012105. doi:10.1063/1.4775351

Raoux S, Rettner CT, Jordan-Sweet JL, Kellock AJ, Topuria T, Rice PM, Miller DC (2007) Direct observation of amorphous to crystalline phase transitions in nanoparticle arrays of phase change materials. J Appl Phys 102:8. doi:10.1063/1.2801000

Simpson RE, Krbal M, Fons P, Kolobov AV, Tominaga J, Uruga T, Tanida H (2010) Toward the ultimate limit of phase change in $Ge_2Sb_2Te_5$. Nano Lett 10:414–419. doi:10.1021/nl902777z

Skelton JM, Lee TH, Elliott SR (2012) Structural, dynamical, and electronic properties of transition metal-doped $Ge_2Sb_2Te_5$ phase-change materials simulated by ab initio molecular dynamics. Appl Phys Lett 101: 024106. doi:10.1063/1.4736577

Stoykovich MP, Nealey PF (2006) Block copolymers and conventional lithography. Mater Today 9:20–29. doi:10.1016/S1369-7021(06)71619-4

Tan CC et al (2013) Compositionally matched nitrogen-doped $Ge_2Sb_2Te_5$/$Ge_2Sb_2Te_5$ superlattice-like structures for phase change random access memory. Appl Phys Lett 103:133507. doi:10.1063/1.4823551

Thelander E, Gerlach JW, Ross U, Lotnyk A, Rauschenbach B (2014) Low temperature epitaxy of Ge-Sb-Te films on BaF_2 (111) by pulsed laser deposition. Appl Phys Lett 105:5. doi:10.1063/1.4903489

Tseng RJ, Tsai CL, Ma LP, Ouyang JY (2006) Digital memory device based on tobacco mosaic virus conjugated with nanoparticles. Nat Nanotechnol 1:72–77. doi:10.1038/nnano.2006.55

Wang RP, Choi DY, Rode AV, Madden SJ, Luther-Davies B (2007) Rebonding of Se to as and Ge in $Ge_{33}As_{12}Se_{55}$ films upon thermal annealing: evidence from x-ray photoelectron spectra investigations. J Appl Phys 101: 4. doi:10.1063/1.2737785

Wang J, Zhao HL, Yang Q, Wang CM, Lv PP, Xia Q (2013) $Li_4Ti_5O_{12}$-TiO_2 composite anode material for lithium-ion batteries. J Power Sources 222:196–201. doi:10.1016/j.jpowsour.2012.08.082

Wong HSP et al (2010) Phase change memory. Proc IEEE 98: 2201–2227. doi:10.1109/jproc.2010.2070050

Yang KY, Hong SH, Kim DK, Cheong BK, Lee H (2007) Patterning of $Ge_2Sb_2Te_5$ phase change material using UV nano-imprint lithography. Microelectron Eng 84:21–24. doi:10.1016/j.mee.2006.07.004

Yoon HR, Jo W, Cho E, Yoon S, Kim M (2006) Microstructure and optical properties of phase-change Ge-Sb-Te nanoparticles grown by pulsed-laser ablation. J Non-Cryst Solids 352: 3757–3761. doi:10.1016/j.jnoncrysol.2006.05.038

Zeng B, Chen XH, Tang QX, Chen CS, Hu AP (2014) Ordered mesoporous necklace-like ZnS on graphene for use as a high performance photocatalyst. Appl Surf Sci 308:321–327. doi:10.1016/j.apsusc.2014.04.165

Zhang Y et al (2008) Phase change nanodots patterning using a self-assembled polymer lithography and crystallization analysis. J Appl Phys 104:5. doi:10.1063/1.2981070